

Magnetic field tomography and differential Faraday rotation

C. Horellou^{1*} and A. Fletcher^{2†}

¹ *Department of Earth and Space Sciences, Chalmers University of Technology, Onsala Space Observatory, SE-439 92 Onsala, Sweden*

² *School of Mathematics and Statistics, Newcastle University, Newcastle-upon-Tyne NE1 7RU, U.K.*

Accepted 201x. Received 201x; in original form 2014 January

ABSTRACT

Wide-band radio polarization observations offer the possibility to recover information about the magnetic fields in synchrotron sources, such as details of their three dimensional configuration, that has previously been inaccessible. The key physical process involved is the Faraday rotation of the polarized emission in the source (and elsewhere along its propagation path). In order to proceed reliable methods are required for inverting the signals observed in wavelength space into useful data in Faraday space, with robust estimates of their uncertainty. In this paper we examine how variations of the intrinsic angle of polarized emission χ_0 with the Faraday depth ϕ within a source affect the observable quantities. Using simple models for the Faraday dispersion $F(\phi)$ and $\chi_0(\phi)$, along with the current and planned properties of the main radio interferometers, we demonstrate how degeneracies among the parameters describing the magneto-ionic medium can be minimised by combining observations in different wavebands. In particular we show that it may be possible to recover the sign (and maybe even the magnitude) of the helicity of the magnetic field.

Key words: polarization – galaxies: magnetic fields – ISM: magnetic fields – radio continuum: galaxies – methods: data analysis – techniques: polarimetric

1 INTRODUCTION

A new generation of radio telescopes will map the polarization of cosmic radio sources over a large range of wavelengths, from a few centimetres to several metres. Since the plane of polarization of a linearly polarized wave is rotated by an amount that depends on the magnetic field and free-electron distributions and the wavelength-squared (λ^2) the resulting data will probe both the synchrotron-emitting sources and any intervening magneto-ionic medium in unprecedented detail. A useful way to characterize the intrinsic properties of magneto-ionic media is to try to reconstruct the Faraday dispersion function, $F(\phi)$, which contains information on the transverse orientation of the magnetic field (B_{\perp}) and on the intrinsic polarized emission as a function of Faraday depth, ϕ . The Faraday depth is proportional to the integral along the line of sight z of the product of the density of thermal electrons and the parallel component of the magnetic field:

$$\phi(z) \propto \int_0^z n_e(z') B_{\parallel}(z') dz', \quad (1)$$

hence, in principle, $F(\phi)$ can be used to obtain both the perpendicular and the parallel components of the three dimensional magnetic field.

Reconstruction of $F(\phi)$ is usually done by taking advantage of the Fourier relationship between the observed polarized emission and the Faraday dispersion function. The *observed* complex polarization $P(\lambda^2)$ can be expressed as the integral over all Faraday depths of the *intrinsic* complex polarization $F(\phi)$ modulated by the Faraday rotation (Burn 1966):

$$P(\lambda^2) = \int_{-\infty}^{+\infty} F(\phi) e^{2j\phi\lambda^2} d\phi \quad (2)$$

so that $F(\phi)$ can be expressed in a similar way:

$$F(\phi) = \frac{1}{\pi} \int_{-\infty}^{+\infty} P(\lambda^2) e^{-2j\phi\lambda^2} d\lambda^2. \quad (3)$$

$F(\phi)$ is usually a complex-valued function:

$$F(\phi) = |F(\phi)| e^{2j\chi_0(\phi)} \quad (4)$$

where $|F(\phi)|d\phi$ is the fraction of polarized flux that comes from regions of Faraday depth between ϕ and $\phi + d\phi$. χ_0 is the intrinsic polarization angle (perpendicular to the transverse component of the magnetic field) and may itself depend on ϕ .

* E-mail: cathy.horellou@chalmers.se

† andrew.fletcher@ncl.ac.uk.

Equation (3) lies at the heart of attempts to recover $F(\phi)$ from multi-frequency observations of the complex polarized intensity (called Rotation Measure synthesis, Brentjens & de Bruyn 2005). The RM synthesis method has been used to recover Faraday components of compact sources (e.g. Mao et al. 2010) and diffuse structures in the Milky Way (e.g. Schnitzeler, Katgert, & de Bruyn 2009), in nearby external galaxies (e.g. Heald, Braun, & Edmonds 2009) and in galaxy clusters (e.g. Pizzo et al. 2011). Several techniques have been proposed to deal with the limited λ^2 coverage provided by real telescopes (RM-CLEAN, Heald 2009; sparse analysis and compressive sensing, Li et al. 2011, Andreut, Stil, & Taylor 2012; multiple signal classification, Andreut 2013) and with the missing negative λ^2 (e.g. using wavelet transforms, Frick et al. 2010, 2011, Beck et al. 2012). Because of the difficulty of the RM synthesis technique to recover multiple Faraday components, it has been suggested to use direct $q(\lambda^2)$ and $u(\lambda^2)$ fitting, where q and u are the ratios of the Q and U Stokes parameters to the total intensity I (Farnsworth, Rudnick, & Brown 2011, O’Sullivan et al. 2012).

In this paper we show how observations, performed in the different wavelength ranges available at existing and planned radio telescopes, can be used to constrain the variation of χ_0 (and therefore the orientation of the magnetic field component perpendicular to the line of sight) with ϕ . We use a Fisher matrix analysis to quantify the precision that can be achieved for fitted parameters and investigate the degeneracies that exist between the different constituents of our model. Recently, Ideguchi et al. (2013) performed a similar analysis to evaluate the capability of new radio telescopes to constrain the properties of intergalactic magnetic fields through observations of background polarized sources. Their work assumed two Faraday components, each with a constant χ_0 , a narrow one (the compact radio source) and a broad one (possibly associated with the Milky Way). Here we consider a linear variation of χ_0 with ϕ and show how the degeneracies between pairs of model parameters can be broken using complementary datasets from different instruments in order to recover $\chi_0(\phi)$, using two simple models of $F(\phi)$, a top-hat and a Gaussian.

In the simple cases we consider, the variation of $\chi_0(\phi)$ corresponds to a helical magnetic field. Magnetic helicity is a natural consequence of dynamo action and sophisticated statistical methods have been devised to try to infer its presence, although without inclusion of Faraday effects (Oppermann et al. 2011, Junklewitz & Enßlin 2011). Anomalous depolarization (an increase rather than the usual decrease of the degree of polarization with wavelength) produced by an helical field was discussed by Sokoloff et al. (1998). Helical fields have been invoked to explain the anomalous depolarization properties of the nearby galaxy NGC 6946 (Urbanik, Elstner, & Beck 1997) and polarization characteristics of the central part of the starburst galaxy NGC 253 (Heesen et al. 2011). The signatures of bi-helical fields are discussed in a recent paper by Brandenburg & Stepanov (2014).

2 ANALYSIS

2.1 Observables

We consider observations of the Stokes parameters Q and U with the instruments listed in Table 1. We scaled the sensitivities σ_{lit} quoted in the literature for a given effective bandwidth BW_{lit} and integration time t_{lit} to new values of the channel width $\Delta\nu$ and integration time t_{int} , as given in the table, assuming that a number of tunings N_{tunings} is needed to cover the whole bandwidth:

$$\sigma = \sigma_{\text{lit}} \sqrt{\frac{BW_{\text{lit}}}{\Delta\nu} \frac{t_{\text{lit}}}{t_{\text{int}}} N_{\text{tunings}}}. \quad (5)$$

The Jansky Very Large Array (JVLA) will be used to carry out sensitive surveys of large parts of the sky. We use figures provided by Steven T. Myers (NRAO) in the Karl Jansky VLA Sky Survey Prospectus (see Table 1) for the JVLA in its B-configuration. In the S-band (2–4 GHz), the effective bandwidth (free from radio frequency interferences) is 1500 MHz, and a noise level of 0.1 mJy can be achieved in 7.7 seconds. The size of the synthesized beam is $2.7''$ at the centre of the band. In the L-band (1–2 GHz), the effective bandwidth is 600 MHz and a noise level of 0.1 mJy can be achieved in 37 seconds of integration. The size of the synthesized beam is $5.6''$. In both cases we assumed a single tuning. We note that Mao et al. (2014) recently submitted a science white paper for a JVLA sky survey in S-band (in the C-configuration), in which they consider several alternatives ranging from a shallow all-sky survey to ultra-deep fields of a few tens of square degrees. They estimate that a shallow all-sky survey of a total of about 3000 hours would lead to the detection of over 2×10^5 polarized sources.

According to the Australian Square Kilometre Array Pathfinder (ASKAP) website a continuum sensitivity of 29 to 37 $\mu\text{Jy}/\text{beam}$ for beams between $10''$ and $30''$ can be reached in 1 hour for a bandwidth of 300 MHz. Four tunings would be required to cover the whole frequency band from 700 to 1800 MHz, so in a total of 1 hour a noise level of 1–1.3 mJy per 1 MHz channel would be reached.

In its first phase, the Square Kilometre Array (SKA) will observe at low frequencies (50 – 350 MHz), mid-frequencies (350 MHz – 3.05 GHz) and in a survey mode in the 650 MHz – 1.67 GHz range (SKA1-Survey). The sensitivity of the SKA1-Survey is expected to be around 263 μJy per 0.1 MHz channel in 1 hour of observation. Since the maximum bandwidth is 500 MHz, two tunings will be needed to cover the entire band.

For the Giant Meterwave Radio Telescope (GMRT) 610 MHz band, our sensitivity estimate is based on the figures quoted by Farnes, Green, & Kantharia (2013) who reached a noise level in Q and U of 36 μJy per beam of $24''$ in 180 minutes in a 16 MHz band centered at 610 MHz. Four tunings would be required to cover the whole band.

According to the GMRT user’s manual the system temperature at 325 MHz is similar to that in the 610 MHz band (106 K versus 102 K). Although the whole band could be covered in only 3 tunings, we assume here a sensitivity of the same order as that achievable in the 610 MHz band.

The high-band array (HBA) of the LOw Frequency ARray (LOFAR) operates at frequencies between 110 MHz and 250 MHz with a filter between 190 and 210 MHz. At the LOFAR frequencies depolarization is extremely strong and

Table 1. Frequency range and sensitivity of the listed instruments. More details are given in Sect. 2.1.

Instrument	Frequency band [MHz]	Sensitivity [mJy]	Channel width [MHz]	Integration	Reference
JVLA S-band	2000-4000	0.3	2	10 min	(1)
JVLA L-band	1000-2000	0.6	1	10 min	(1)
ASKAP	700–1800	2.5	1	10 min	(2)
SKA1-Survey	650–1670	0.3	1	10 min	(3)
GMRT high	580–640	0.5	1	1 hr	(4)
GMRT low	305–345	0.5	1	1 hr	(4)
LOFAR HBA2	210–250	0.5–1.1	4	8 hr	(5)
LOFAR HBA1	110–190	0.3	4	8 hr	(5)

(1) https://science.nrao.edu/science/surveys/vlass/VLASKySurveyProspectus_WP.pdf(2) www.atnf.csiro.au/projects/askap/spec.html(3) https://www.skatelescope.org/wp-content/uploads/2013/03/SKA-TEL-SK0-DD-001-1_BaselineDesign1.pdf, page 18.(4) www.ncra.tifr.res.in/ncra/gmrt/gmrt-users(5) <https://www.astron.nl/radio-observatory/astronomers/lofar-imaging-capabilities-sensitivity/sensitivity-lofar-array/sensiti>, Table 4, for a 40-station Dutch array. Those numbers are preliminary, especially in the highest band.

the measurements at the quoted sensitivities do not provide valuable constraints on the parameters related to the magnetic field. The LOFAR frequency coverage is displayed in Fig. 1 but the LOFAR confidence intervals are therefore not shown in the other figures.

2.2 Fisher analysis

The Fisher analysis method is often used in cosmology (e.g. Albrecht et al. 2006, page 94). Consider a set of N data points and a model with P parameters, p_1, \dots, p_P . The Fisher matrix is proportional to the second partial derivatives with respect to two given parameters of the likelihood function \mathcal{L} that the data set derives from the given model. If the measurement errors follow a Gaussian probability distribution, then

$$\mathcal{F}_{jk} = -\frac{\partial^2 \ln \mathcal{L}}{\partial p_j \partial p_k} = \frac{1}{2} \frac{\partial^2 \chi^2}{\partial p_j \partial p_k} \quad (6)$$

where χ^2 is defined in the standard way. Denoting Q_{mod} and U_{mod} the values of the Stokes parameters Q and U for the assumed model, estimated at wavelengths λ_i and noise levels σ_i , we have

$$\chi^2 = \sum_{i=1}^N \left(\frac{Q_i - Q_{\text{mod}}(\lambda_i; p_1, \dots, p_P)}{\sigma_i} \right)^2 + \left(\frac{U_i - U_{\text{mod}}(\lambda_i; p_1, \dots, p_P)}{\sigma_i} \right)^2. \quad (7)$$

The Fisher matrix can be written as

$$\mathcal{F}_{jk} = \sum_{i=1}^N \frac{1}{\sigma_i^2} \left(\frac{\partial Q_{\text{mod}}(\lambda_i^2; p_1, \dots, p_P)}{\partial p_j} \frac{\partial Q_{\text{mod}}(\lambda_i^2; p_1, \dots, p_P)}{\partial p_k} + \frac{\partial U_{\text{mod}}(\lambda_i^2; p_1, \dots, p_P)}{\partial p_j} \frac{\partial U_{\text{mod}}(\lambda_i^2; p_1, \dots, p_P)}{\partial p_k} \right). \quad (8)$$

The covariance matrix is the inverse of the Fisher matrix:

$$\sigma_{jk}^2 = (\mathcal{F}^{-1})_{jk}. \quad (9)$$

2.3 Models of $F(\phi)$ with linearly varying intrinsic polarization angle

We consider two simple models for $F(\phi)$, each with a linearly varying χ_0 as a function of Faraday depth:

$$\chi_0(\phi) = \alpha + \beta\phi. \quad (10)$$

This is a parametrisation of χ_0 as a first-order polynomial and, as discussed below, it can also be interpreted as a helical magnetic field.

2.3.1 Top-hat Faraday dispersion function

One of the simplest possible models for $F(\phi)$ is the top-hat,

$$F(\phi; \mathbf{p}) = F_0 T(\phi; \mathbf{p}) e^{2j\chi_0(\phi; \mathbf{p})} \quad (11)$$

where the set of parameters $\mathbf{p} \in \{F_0, \phi_0, \phi_m, \alpha, \beta\}$, $\chi_0(\phi; \mathbf{p})$ is given by Eq. (10) and $T(\phi; \mathbf{p})$ is the top-hat function, with $T = 1$ in the range $\phi_0 - \phi_m < \phi < \phi_0 + \phi_m$ and $T = 0$ elsewhere. The complex polarization is

$$P(\lambda^2; \mathbf{p}) = 2\phi_m F_0 \text{sinc}[2\phi_m(\lambda^2 + \beta)] e^{2j\chi(\lambda^2; \mathbf{p})} \quad (12)$$

where

$$\chi(\lambda^2; \mathbf{p}) = \alpha + (\lambda^2 + \beta)\phi_0. \quad (13)$$

In a uniform slab, the Faraday depth varies linearly with the z -coordinate for ϕ between $\phi_0 \pm \phi_m$:

$$\phi = 0.81n_e B_{\parallel} z \quad (14)$$

where n_e is in cm^{-3} , B_{\parallel} in μG , z in pc and ϕ in rad m^{-2} .

Consider a magnetic field constant along the line of sight, but with a rotating component on the plane of the sky:

$$B = \begin{pmatrix} B_{\perp} \cos(\alpha + k_H z) \\ B_{\perp} \sin(\alpha + k_H z) \\ B_{\parallel} \end{pmatrix}. \quad (15)$$

The intrinsic polarization angle clearly varies with the Faraday depth:

$$\chi_0 = \alpha + k_H z = \alpha + \beta\phi \quad (16)$$

where

$$\beta = \frac{k_H}{0.81n_e B_{\parallel}}. \quad (17)$$

This can be written in a more convenient way, using order-of-magnitude values for the electron density and the magnetic field in the interstellar medium:

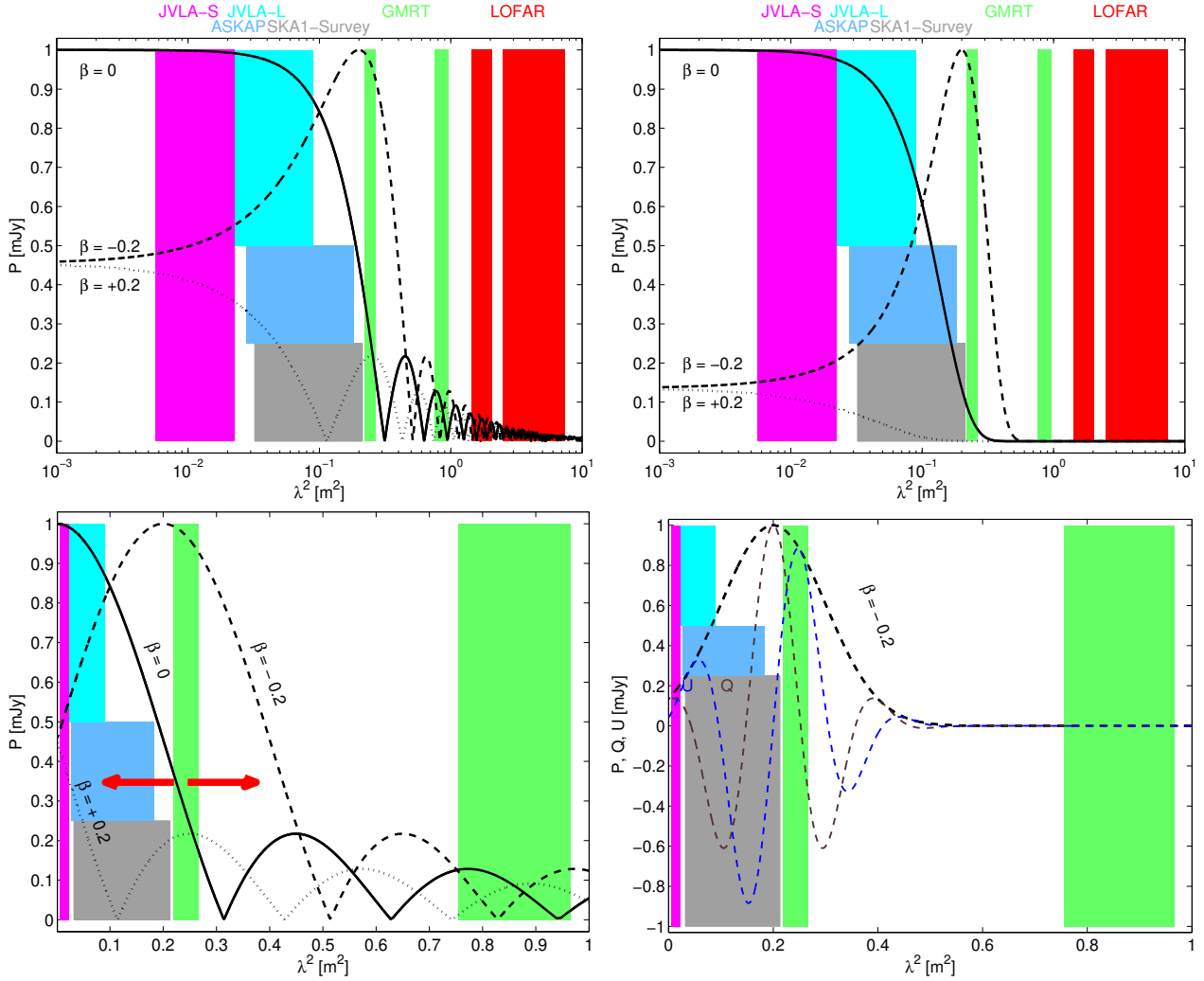


Figure 1. Polarized intensity versus λ^2 for the top-hat model of the Faraday dispersion function (left) and the Gaussian model (right) for different values of the β parameter: $\beta = 0$ (solid line), $\beta = -0.2 \text{ m}^2$ (dashed line), and $\beta = +0.2 \text{ m}^2$ (dotted line). The graphs on the top row are in semilogarithmic scale and extend out to the frequency bands of LOFAR, while the graphs on the bottom row are in linear scale and extend to a wavelength of about 1 metre, a band covered by the GMRT. The wavebands of several instruments are shown in colour. For the Gaussian model, the variations of the Stokes parameters Q and U are also shown (bottom right panel, brown and blue dashed lines) for the case with $\beta = -0.2 \text{ m}^2$. The pattern of polarized intensity is shifted horizontally as β varies, peaking at $\lambda^2 = -\beta$, as illustrated by the red arrows in the bottom left panel. A negative β (B_{\parallel} and handedness of B_{\perp} of opposite signs) results in a peak at $\lambda^2 > 0$, whereas a positive β results in increased depolarisation due to the combined depolarization effects of intrinsic helicity and Faraday rotation.

$$\frac{\beta}{\text{m}^2} = 0.086 \left(\frac{k_H}{2\pi \text{ rad kpc}^{-1}} \right) \left(\frac{0.03 \text{ cm}^{-3}}{n_e} \right) \left(\frac{3\mu\text{G}}{B_{\parallel}} \right) \quad (18)$$

For an helical field with $k_H \simeq 2\pi \text{ rad kpc}^{-1}$, the β parameter will be around 0.1 m^2 .

Note that the sign of β depends on the relative orientation of the magnetic field component along the line of sight and the handedness of the helix. A positive β means that B_{\parallel} , which produces the Faraday rotation, and the intrinsic rotation of B_{\perp} have the same direction. A negative β means that the Faraday rotation effectively counteracts the intrinsic rotation of the plane-of-sky magnetic field. This effect will be discussed further in Sect. 3.

2.3.2 Gaussian Faraday dispersion function

As a simple alternative to the top-hat parametrisation of $F(\phi)$ we also consider a Gaussian model,

$$F(\phi; \mathbf{p}) = F_0 \exp \left[-0.5 \left(\frac{\phi - \phi_0}{\sigma_{\phi}} \right)^2 \right] e^{2j\chi_0(\phi; \mathbf{p})} \quad (19)$$

where \mathbf{p} and $\chi_0(\phi, \mathbf{p})$ are defined as before. This gives a complex polarization of

$$P(\lambda^2; \mathbf{p}) = \sqrt{2\pi}\sigma_{\phi} F_0 \exp \left[-0.5 \left(\frac{\lambda^2 + \beta}{(2\sigma_{\phi})^{-1}} \right)^2 \right] e^{2j\chi(\lambda^2; \mathbf{p})} \quad (20)$$

where $\chi(\lambda^2; \mathbf{p})$ is again given by Eq. (13). The modulus of $P(\lambda^2)$ is a Gaussian centered on $\lambda^2 = -\beta$ with variance $\sigma^2 = (2\sigma_\phi)^{-2}$.

2.3.3 General case

In the two previous Sections we calculated $P(\lambda^2)$ by integrating Eq. (2) analytically. Using the properties of the Fourier transforms, we now show why any linear variation of χ_0 with ϕ produces a translation in λ^2 space of the observed polarized intensity.

Using the standard expression for Fourier transform (integral over t of a function $f(t)$ times $e^{-2\pi j\nu t}$ for the direct transform and times $e^{2\pi j\nu t}$ for its inverse), Eq. (2) can be written as

$$P(\pi\lambda^2) = FT^{-1}\{F(\phi)\} \quad (21)$$

where FT^{-1} is the inverse Fourier transform.

Using $F(\phi) = F_c(\phi - \phi_0)$ to have a function centered at $\phi = \phi_0$,

$$P(\pi\lambda^2) = FT^{-1}\{F_c(\phi - \phi_0)|e^{2j(\alpha + \beta\phi)}\}. \quad (22)$$

The factor $e^{2j\alpha}$ is independent on ϕ and can be taken out of the integral. Multiplication becomes a convolution in Fourier (λ^2) space and so

$$P(\pi\lambda^2) = e^{2j\alpha} FT^{-1}\{|F_c(\phi - \phi_0)|\} * FT^{-1}\{e^{2j\beta\phi}\}. \quad (23)$$

The translation in ϕ -space gives a rotation in λ^2 -space, and the inverse transform of the term involving $\beta\phi$ becomes a delta-function, giving

$$P(\pi\lambda^2) = e^{2j\alpha} \left(e^{2j\pi\phi_0\lambda^2} FT^{-1}\{|F_c(\phi)|\} \right) * \delta\left(\lambda^2 + \frac{\beta}{\pi}\right). \quad (24)$$

We then obtain

$$\begin{aligned} P(\pi\lambda^2) &= e^{2j\pi\phi_0(\lambda^2 + \frac{\beta}{\pi})} \left(FT^{-1}\{|F_c(\phi)|e^{2j\alpha}\} * \delta\left(\lambda^2 + \frac{\beta}{\pi}\right) \right) \\ &= e^{2j\pi\phi_0(\lambda^2 + \frac{\beta}{\pi})} P_{\beta=0}(\pi(\lambda^2 + \frac{\beta}{\pi})) \end{aligned} \quad (25)$$

where $P_{\beta=0}$ is the complex polarization corresponding to $F_c(\phi)$ when $\beta = 0$. Changing variable from $\pi\lambda^2$ to λ^2 , we obtain

$$P(\lambda^2) = e^{2j\pi\phi_0(\lambda^2 + \beta)} P_{\beta=0}(\lambda^2 + \beta), \quad (26)$$

so that

$$|P(\lambda^2)| = |P_{\beta=0}(\lambda^2 + \beta)|. \quad (27)$$

This shows that the observed modulus of the polarized intensity of a medium with a given β is simply a translation by β in λ^2 space of what would be observed if β were equal to zero.

$|F_c(\phi)|$ is real-valued, by definition; if it is even, then its inverse Fourier transform is also real-valued, and the observed polarization angle will be

$$\chi(\lambda^2) = \alpha + \phi_0(\lambda^2 + \beta) \quad (28)$$

as found in Sect. 2.3.1 and 2.3.2 for the top-hat and the Gaussian cases.

3 RESULTS

We use a fiducial top-hat model of the Faraday dispersion function with the following parameters: $\phi_0 = 15 \text{ rad m}^{-2}$,

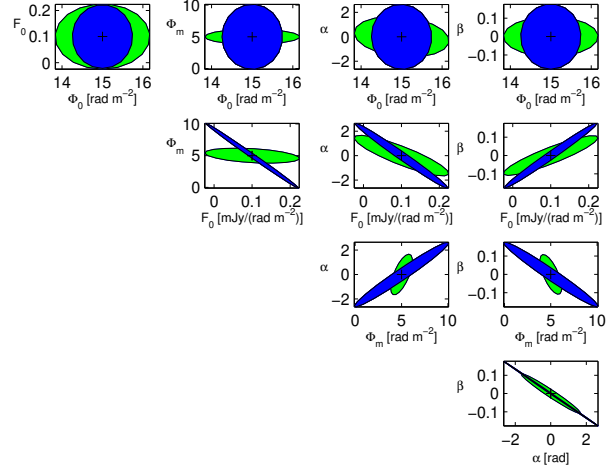


Figure 2. 68.3% confidence regions for a top-hat model of the Faraday dispersion function when $\beta = 0$. The ASKAP regions are in blue and the GMRT ones in green.

$\phi_m = 5 \text{ rad m}^{-2}$, $F_0 = 0.1 \text{ mJy / (rad m}^{-2})$, $\alpha = 0 \text{ rad}$, and three values of the β parameter, 0 and $\pm 0.2 \text{ m}^2$. For comparison, we also use a Gaussian model of $|F(\phi)|$ with the same total flux (1 mJy). The dispersion of the Gaussian is $\sigma_\phi = 1 \text{ rad m}^{-2}$ and the peak flux density per unit of Faraday depth $F_0 = 1/\sqrt{2\pi} \simeq 0.4 \text{ mJy / (rad m}^{-2})$.

Figure 1 shows the variation of the polarized intensity with λ^2 for a top-hat (left column) and a Gaussian model (right column) of the Faraday dispersion function. In the top-hat case, the solid line ($\beta = 0$) is the well-known sinc function produced by a uniform slab, which is more usually shown using the linear horizontal axis used in the bottom left panel. In the Gaussian case the polarized intensity decreases monotonically and no emission is produced in the longer wavebands at which the GMRT and LOFAR operate. In the bottom right panel we show the variation of the Q and U Stokes parameters (in brown and blue) for the Gaussian $F(\phi)$, which are the direct observables. They oscillate with a 90 degrees phase with respect to each other.

In the rest of the paper we focus on the top-hat model because it gives stronger emission in longer wavebands for the parameters selected here and it includes the standard case for Faraday depolarization calculations of a uniform slab. It is most interesting to compare the variations of the polarized intensity for a positive and a negative β . When $\beta > 0$, the intrinsic helicity of the magnetic field and the Faraday rotation act in the same direction. This results in an increased depolarization at short wavelengths. Even for $\lambda = 0$, where Faraday depolarization is absent, the emission is significantly depolarized compared to the case of a constant magnetic field orientation ($\beta = 0$). When $\beta < 0$, Faraday rotation counteracts the intrinsic rotation of the field, which means that the polarized emission peaks at a wavelength different from zero (dashed lines), where $\lambda^2 = -\beta$ (eqs. (12) and (20)). This effect is similar to the ‘‘anomalous depolarisation’’ discussed in Sokoloff et al. (1998, Section 9).

Figure 2 shows the 68.3% confidence regions of the five different parameters obtained from the Fisher analysis for $\beta = 0$. The colour code is the same as in Fig. 1, with the ASKAP confidence regions in blue and the GMRT

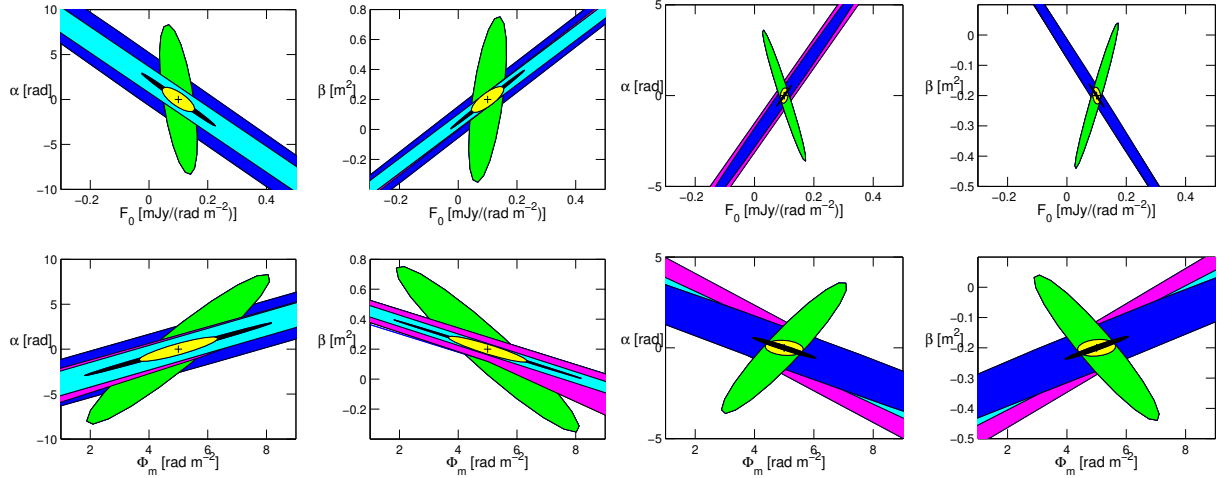


Figure 3. 68.3% confidence regions for a top-hat model of the Faraday dispersion function. The colour code is the same as in Fig. 1. Left panel (four figures): $\beta = +0.2 \text{ m}^2$; right panel (four figures): $\beta = -0.2 \text{ m}^2$. The yellow ellipses show the confidence regions obtained by combining an ASKAP (blue ellipses) and a GMRT (green ellipses) data set. The SKA1-Survey confidence ellipses are shown in black.

ones in green. The plots on the first row show that the central Faraday depth ϕ_0 is mostly uncorrelated with the other parameters. On the other hand, the ϕ_m parameter, which describes the extent of the Faraday component in ϕ -space, is strongly correlated with the parameters related to the intrinsic polarization angle (α and β) and at short wavelengths (in the ASKAP band) with the normalization of $F(\phi)$ (F_0). This is because the crucial effect is Faraday *differential* rotation across the Faraday component and not the magnitude of the central Faraday depth. An increase in ϕ_m means stronger depolarization due to differential rotation which must be counteracted by a more negative β in order to produce a similar fit to the data. Vice-versa, a lower ϕ_m means weaker depolarization and β needs to become positive to increase the depolarization. In other words ϕ_m and β are anti-correlated around $\beta = 0$. Most importantly, the strength of the correlation between pairs of parameters including α or β varies with the selected waveband. This is what makes it possible to break parameter degeneracies by combining short-wavelength (type ASKAP) and long wavelength (type GMRT) data sets in order to better constrain the derived parameter values, as we discuss next.

Figure 3 shows the one-sigma confidence ellipses for the α and β parameters in relation with F_0 and ϕ_m for positive ($\beta = +0.2 \text{ m}^2$, four left panels) and negative β 's ($\beta = -0.2 \text{ m}^2$, four right panels). The colour code is the same as in Fig. 1. As expected, the orientation of the ellipses is similar for the short-wavelength JVLA, ASKAP and SKA1-Survey. On the other hand, the long-wavelength GMRT data set produces a different correlation between parameters; in some cases the confidence ellipses at short and long wavelengths are almost orthogonal, making it possible to shrink the confidence intervals on the derived parameter values considerably by using both wavelength ranges together. This is further illustrated in Fig. 4 where the precision that can be achieved on the β parameter for different instruments is shown. A combination of ASKAP and GMRT observations makes it possible to reach an uncertainty $\Delta\beta < 0.25 \text{ m}^2$ if $\beta < 0$, for the integration times shown in Table 1 and the set of model parameters used. If

$\beta > 0$, all signals are weaker because of increased depolarization and the precision on β (and all other model parameters) is lower.

4 SUMMARY

We examined how variations of the intrinsic polarization angle χ_0 with the Faraday depth ϕ within a source affect the observable quantities. Using simple models for the Faraday dispersion $F(\phi)$ and $\chi_0(\phi)$, along with the current and planned properties of the main radio interferometers, we show how degeneracies among the parameters describing the magneto-ionic medium can be minimised by combining observations in different wavebands. In particular we have shown that it may be possible to recover the sign and the magnitude of β , a parameter that we have defined and that is related to the relative effect of the helicity of the transverse magnetic field and the Faraday rotation due to the parallel component of the magnetic field. Since the direction of B_{\parallel} can be easily inferred from RM measurements, it should be possible to recover the sign (and, under some assumptions the magnitude) of the helicity of the magnetic field. This approach is complementary to statistical studies of the correlation between the degree of polarization and the rotation measures of cosmic sources which may also provide information on magnetic helicity (Volegova & Stepanov 2010, Brandenburg & Stepanov 2014).

Planned surveys of fixed sensitivity will be biased towards radio sources with negative β 's, because of the depolarization produced by positive β 's. Detection of positive β 's will be more difficult both through $Q(\lambda^2)$ and $U(\lambda^2)$ model-fitting and RM synthesis because most of the signal is shifted toward negative λ^2 . Brandenburg & Stepanov (2014) show that restricting the integral in Eq. (3) to the positive λ^2 yields an erroneous reconstruction of $F(\phi)$.

In this work we used a first-order parametrisation of the variation of intrinsic polarization angle with Faraday depth. Higher order representations could be used (or e.g. Chebyshev polynomials) if the data are of sufficient quality.

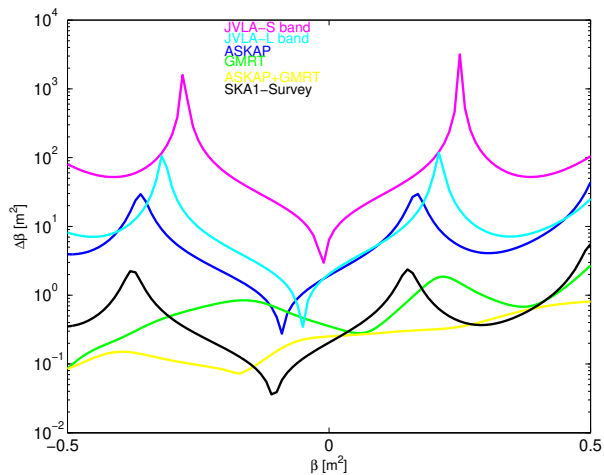


Figure 4. Precision that can be achieved on the β parameter as a function of β for observations with the instruments in Table 1. The combination of ASKAP and GMRT (shown here in yellow) provides the smallest dependence of the uncertainty on β .

Including a second-order term implies a convolution with an imaginary Gaussian and a significantly more complicated expression of $P(\lambda^2)$.

ACKNOWLEDGMENTS

We thank Oliver Gressel for organising the stimulating Nordita workshop “Galactic Magnetism in the Era of LO-FAR and SKA” held in Stockholm in September 2013. We also thank Axel Brandenburg and Rodion Stepanov for interesting discussions on the topics discussed in this paper and for sharing their related results with us. AF is grateful to the Leverhulme Trust for financial support under grant RPG-097.

REFERENCES

- Albrecht A., et al., 2006, *astro*, arXiv:astro-ph/0609591
 Andrecut M., 2013, *MNRAS*, 430, L15
 Andrecut M., Stil J. M., Taylor A. R., 2012, *AJ*, 143, 33
 Beck R., Frick P., Stepanov R., Sokoloff D., 2012, *A&A*, 543, A113
 Brandenburg A., Stepanov R., 2014, *ApJ*, submitted
 Brentjens M. A., de Bruyn A. G., 2005, *A&A*, 441, 1217
 Burn B. J., 1966, *MNRAS*, 133, 67
 Farnes J. S., Green D. A., Kantharia N. G., 2013, arXiv, arXiv:1309.4646
 Farnsworth D., Rudnick L., Brown S., 2011, *AJ*, 141, 191
 Frick P., Sokoloff D., Stepanov R., Beck R., 2011, *MNRAS*, 414, 2540
 Frick P., Sokoloff D., Stepanov R., Beck R., 2010, *MNRAS*, 401, L24
 Heald G., Braun R., Edmonds R., 2009, *A&A*, 503, 409
 Heald G., 2009, *IAUS*, 259, 591
 Heesen V., Beck R., Krause M., Dettmar R.-J., 2011, *A&A*, 535, A79
 Ideguchi S., Takahashi K., Akahori T., Kumazaki K., Ryu D., 2013, arXiv, arXiv:1308.5696

- Junklewitz H., Enßlin T. A., 2011, *A&A*, 530, A88
 Li F., Brown S., Cornwell T. J., de Hoog F., 2011, *A&A*, 531, A126
 Mao S. A., Gaensler B. M., Haverkorn M., Zweibel E. G., Madsen G. J., McClure-Griffiths N. M., Shukurov A., Kronberg P. P., 2010, *ApJ*, 714, 1170
 Mao S. A., et al., 2014, arXiv, arXiv:1401.1875
 O’Sullivan S. P., et al., 2012, *MNRAS*, 421, 3300
 Oppermann N., Junklewitz H., Robbers G., Enßlin T. A., 2011, *A&A*, 530, A89
 Pizzo, R. F., de Bruyn, A. G., Bernardi, G., Brentjens, M. A. 2011, *A&A*, 525, A104
 Schnitzeler D. H. F. M., Katgert P., de Bruyn A. G., 2009, *A&A*, 494, 611
 Sokoloff D. D., Bykov A. A., Shukurov A., Berkhuijsen E. M., Beck R., Poezd A. D., 1998, *MNRAS*, 299, 189
 Urbanik M., Elstner D., Beck R., 1997, *A&A*, 326, 465
 Volegova A. A., Stepanov R. A., 2010, *JETPL*, 90, 637